

NeuroHSMD: Neuromorphic Hybrid Spiking Motion Detector

Pedro Machado , Eiman Kanjo , Andreas Oikonomou  and Ahmad Lotfi 

Department of Computer Science
Clifton Lane, Nottingham, NG11 8NS
United Kingdom

Email: {pedro.machado, eiman.kanjo, andreas.oikonomou, ahmad.lotfi}@ntu.ac.uk

Abstract—Vertebrate retinas are highly-efficient in processing trivial visual tasks such as detecting moving objects, yet a complex task for modern computers. The detection of object motion is done by specialised retinal ganglion cells named Object-motion-sensitive ganglion cells (OMS-GC). OMS-GC process continuous signals and generate spike patterns that are post-processed by the Visual Cortex. The Neuromorphic Hybrid Spiking Motion Detector (NeuroHSMD) proposed in this work accelerates the HSMD algorithm using Field-Programmable Gate Arrays (FPGAs). The Hybrid Spiking Motion Detector (HSMD) algorithm was the first hybrid algorithm to enhance dynamic background subtraction (DBS) algorithms with a customised 3-layer spiking neural network (SNN) that generates OMS-GC spiking-like responses. The NeuroHSMD algorithm was compared against the HSMD algorithm, using the same 2012 change detection (CDnet2012) and 2014 change detection (CDnet2014) benchmark datasets. The results show that the NeuroHSMD has produced the same results as the HSMD algorithm in real-time without degradation of quality. Moreover, the NeuroHSMD proposed in this paper was completely implemented in Open Computer Language (OpenCL) and therefore is easily replicated in other devices such as Graphical Processor Units (GPUs) and clusters of Central Processor Units (CPUs).

Index Terms—SNN, HMSD, NeuroHSMD, retinal cells, object motion sensitive ganglion cells, FPGA, background subtraction, object motion detection

I. INTRODUCTION

THE human brain is characterised by its tolerance to faults/noise, concurrent processing capabilities, flexibility and high level of parallelisation when processing data. Furthermore, the adult human brain has a power consumption of about 400 Kcal per day, equivalent to 25 Watts [1]. Again, the human brain can reach 10-50 petaflops outperforming any Commercial-of-the-shelf (COTS) CPU [2]. Despite CPUs outperforming the human brain when processing and transmitting sequential signals in several orders of magnitude, the human brain exceeds CPUs processing millions of signals in parallel using its massively parallel circuits [1], [2].

The human brain is composed of millions of interconnected neuron circuits composed of different types of neuron cells and contributing to specific brain computations [3], [4]. While CPUs transmit signals at a speed of tenths of GHz, the neuronal circuits transmit signals at a rate of hundreds of Hertz [3], [4]. Nevertheless, the human brain can outperform CPUs when processing signals from complex systems such as the

Auditory and Visual systems because of its massive parallel structure [4].

GPUs and FPGAs are devices with parallel processing capabilities that can be used with CPUs for accelerating parallelisable algorithms. GPUs are specialised electronic circuits with a flexible architecture designed for parallel processing of graphics and video rendering and accelerating some types of AI algorithms [5]. FPGAs are integrated circuits composed of built-in interconnected hardware blocks that can be freely reprogrammable after manufacturing [6]. Unlike GPUs with a well-defined architecture, FPGAs are flexible devices that enable the user to describe new hardware architectures, including brain-like, neuromorphic architectures.

Background Subtraction (BS) methods have been studied for the last 30 years [7] and are used to detect and extract the foreground (composed of moving objects) from the background (composed of static or semi-static algorithms). Although object motion detection is a trivial task for vertebrate retinas [8], [9], robust object motion detection is a complex task using BS methods [7]. More recently, BS algorithms have been improved using Machine Learning (ML) algorithms [7]. ML is a research field that focuses on the development of algorithms that mimic the way that humans learn and gradually improve the accuracy and has been around for the last forty years [10]. Among other research topics, ML includes Artificial Neural Networks (ANN) and Spiking Neural Networks (SNN) [11]. ANNs have been widely used for classification and pattern recognition tasks, but at the same time, ANNs lack biological realism. Unlike ANNs that have been studied for more than thirty years, SNNs emerged about twenty years ago and have gained growing interest by researchers because of their biological plausibility [11].

The SNNs are well known for their biological plausibility but also by their complexity inherited from biological systems, which are characterised for being massively parallel [11]. Modern computation platforms rely heavily on Central Processor Units (CPUs) to provide compatibility and security with other devices/applications. Although CPUs have been evolving in recent years, CPUs still rely on the von Neumann architecture proposed by John von Neumann proposed in 1945 [10], [12]. Blank [13] wrote in 2018 that Moore's law which states that the number of transistors in dense Integrated Circuits (ICs) doubles every eighteen to twenty-

four months, has ended around 2008. Furthermore, the clock speed has reached technological limitations preventing CPUs from working with frequencies above 4 GHz, which also introduces memory barriers, and power dissipation challenges [13]. Therefore, the design of the CPU paradigm has shifted into multi-core and multi-processor to overcome the limitations associated with the clock speed [10]. The scientific community agrees that the multi-core and multi-processor strategy will shortly meet technological limitations related to the increase of power consumption of these solutions [10].

Machado et al. proposed the HSMD algorithm [14] that has proven to be very sensitive to object motion events triggered by objects as a direct consequence of using an SNN to emulate the basic functionality observed in OMS-GC (see Figure 1). The SNN utilised is composed of 4 layers of neurons interconnected on a 1:1 synaptic connectivity. SNNs are, by their parallel nature, not optimised for sequential processing architectures such as CPU architectures. FPGAs were the obvious choice for accelerating the SNN in the HSMD algorithm because they offer the flexibility to describe massively parallel architectures. FPGAs are typically reprogrammed using VHDL or Verilog, which are flexible but complex Hardware Description Languages (HDLs). In recent years, the FPGA manufacturers have invested in High Level of Synthesis (HLS) tools to enable Users to reprogram FPGAs using C-like programming languages. One of the most successful HLS tools is the Open Computer Language OpenCL, which allows users to program kernels that can be compiled targeting CPUs, GPUs, and FPGAs.

The NeuroHSMD is the hardware implementation of the HSMD algorithm [14]. As discussed above, FPGAs offer the desired flexibility to accelerate massively parallel SNN architectures. Therefore, a high-end FPGA was selected for accelerating the HSMD's SNN. OpenCL was used for describing the SNN because it provides a higher level of abstraction when compared with HDL and to increase the productivity and compatibility with other OpenCL compatible devices (such as other FPGA devices, GPUs and CPUs). The results show that the NeuroHSMD was 82% faster processing 720×480 than the HSMD algorithm. Furthermore, the NeuroHSMD was ranked first alongside the HSMD when benchmarked against CDnet2012 [15], and CDnet2014 [16] datasets, meaning that there was no degradation of the accuracy.

The paper is structured as follows: the background research is presented in Section II, the hardware platform details are discussed in Section III; the NeuroHSMD architecture is presented in Section IV; the results are presented in Section V and the discussion of the NeuroHSMD results and future work in Section VI.

II. BACKGROUND RESEARCH

Reliable and optimised object motion detection in videos captured from static and/or moving cameras is essential for a wide range of computer vision applications such as video surveillance of humans and animal activities, collision avoidance, advanced driver-assistance systems, etc. [17], [18]. It

is one of the most researched fields in computer vision and has been studied for more than 30 years [7]. Although the first object motion detection models were designed for static cameras, the advances in sensor technology and the accessibility to portable devices fitted with cameras is triggering more challenging scenes with both cameras and objects moving at the same time [7]. Object Motion detection challenges can be summarised as follows [18], [7] :

- **Bootstrapping:** the sequence of images includes objects in both the background and foreground.
- **Camouflage:** the objects in the foreground are either obstructed by background objects or are composed of similar colours.
- **Dynamic background:** the objects in the background include parasitic movements such as surface water movement, branches and leafs shaking in trees, flags on windy days, etc.
- **Camera aperture:** blurred background and foreground as a consequence of the incorrect opening in a lens through which light passes to enter the camera.
- **Variation of illumination:** instant variations of illumination will increase the number of false-positive detections (i.e. pixels that should belong to the background are classified as foreground).
- **Low frame rate:** the temporal distance between image frames prevents instant updates of the background and illumination changes which reduces the accuracy and increases the number of false positives.
- **Motion blur:** caused by rapid camera movements or jittering, which blurs the image.
- **Parallax:** the apparent displacement of an object as a consequence of the camera movement. The Parallax will have implications on the background modelling and its compensation.
- **Moving camera:** moving cameras introduce complexity because the static objects seem to be moving, and objects moving at a similar speed in the same direction of the camera will seem to be static.
- **Background objects movement:** although static objects can be added to and removed from the background, such objects should still be considered static.
- **Night videos:** night videos have dim light, lower contrast and reduced colour information.
- **Noisy images:** low-quality sensors, dust exposure, dirty lens, bright lights and low resolution are examples of factors that cause noisy images.
- **Shadows:** shadows created by objects when exposed to light sources (e.g. sun rays and artificial illumination) should not be part of the foreground models.
- **Stationary foreground objects:** a foreground that has stopped moving for a short period should not become part of the background model;
- **Challenging weather:** weather conditions (such as fog, rainstorms, strong winds, intense sun rays) have a major impact on the image quality and reduce the quality of the image drastically.

Multiple challenges may have to be addressed depending

on the use-case scenario. Garcia et al. and Chapel et al. [7], [18] suggested the following categories of use-case scenarios:

- 1) **Visual analysis of human activities** fixed or movable cameras used for monitoring human activities. Human activities can include highway maintenance (e.g. traffic density estimation, vehicle tracking, detection of dangerous manoeuvres)[19], [20]; tracking people in public places (e.g. airports, train stations, seaports) [21], [22]; monitoring specific people/objects in mass events (e.g. sports games, music concerts, manifestations and gatherings) [23], [24], [25]; and indoor/outdoor behaviour analysis (e.g. track people in closed public spaces, body-cameras installed police forces) [26], [27].
- 2) **Visual observation of animals behaviours** the observation of animals enables one to better understand the health status of individuals and/or colonies of animals. Animals behaviours may include monitoring of livestock (monitor cows, pigs and diseases detection through the analysis of atypical movements) [28], [29]; gathering understanding about complex colonies of insects (e.g. bees and ants have communication mechanisms that enables them to work together to solve complex problems) [30], [31]; and monitoring wildlife (e.g. track movements of shoals of fish or pods of whales) [32], [33].
- 3) **Visual observation of natural environments** the detection of foreign objects in natural environments is crucial for such environments. Some examples of natural environments are forests, lakes, rivers, oceans and glaciers that require active human intervention to protect biodiversity in terms of fauna and flora [34], [35].
- 4) **Visual hull computation** object motion detection is currently being used in many sports (such as Football, Tennis and Athletics) to perform athletes movements analysis [36], [37].
- 5) **Human-machine interface (HMI)** gesture recognition enables users to interact with machines. HMI is currently being used in many fields such as in games (gestures are mapped into game instructions); health (capture of facial motions to enable patients with severe muscular degenerative diseases to communicate using computers); and augmented/virtual reality (enable interaction between users and mixture of real and virtual objects for completing specific tasks) [38].
- 6) **Content-based video coding/decoding** the foreground can be extracted from the background and encoded and streamed to the destination. At the destination, the foreground can be decoded and added to the pre-existing background model [39], [40].
- 7) **Background substitution** state-of-the-art conference platforms enable users to blur or substitute the background in conference calls. The background substitution is being widely used to protect users' privacy [41], [42].
- 8) **Advanced driver-assistant systems (ADAS) and navigational systems (NS)** ADAS/NS require constant updates of the foreground models to ensure that autonomous/semi-autonomous systems can safely navigate without colliding with a multitude of objects and

living beings moving at random speeds and variable trajectories [43], [44].

Consecutive frame difference, background subtraction and optical flow are the main categories for detecting object motion. Consecutive frame difference methods are the simplest to implement and require less computational resources but are also the most sensitive to the challenges listed above [7], [18]. In contrast, optical flow methods are the most robust but require more computational resources and consequently are not suitable for real-time applications. Therefore, Background Subtraction (BS) methods are commonly used methods for splitting the background from the foreground in applications with strict real-time requirements. The target of this Research Programme is focused on real-time or near-real-time application; therefore, the rest of this section will cover background subtraction works in the literature. Nevertheless, the reader will find more details about the consecutive frame difference and/or optical flow methods in the following suggested literature [7], [18].

FPGAs are specialised devices that can be reprogrammable after manufacture and offer high flexibility, high degree of parallelism, high-performance and low-power platforms [45]. FPGA offers the desirable flexibility for accelerating SNNs which are characterised for being massively parallel [46]. FPGAs are also known for being programmed complex low-level hardware description languages such as VHDL, and Verilog [47]. Nowadays, FPGA development has been simplified with the introduction of HLS tools which allow FPGA developers to implement their application using high-level programming languages such as C and OpenCL [47].

Mishra et al. [48] identified in their survey that many of SNN usually have about $10^4 \sim 10^8$ neurons and $10^{10} \sim 10^{14}$ synapses and that high-performance neural hardware is essential for practical application. Li et al. [49] proposed the implementation of visual cortex neurons on FPGAs. The implemented visual cortex neurons exhibited the same dynamics as those recorded from real neurons using multi-electrodes arrays. Li et al.[50] implemented 256 fully connected neurons, and its performance was assessed by storing four patterns and applying similar patterns containing errors. The implemented system was capable of operating using a 100 MHz clock, which enables the acceleration of the system 40 times above the real-time operation [50]. Cassidy et al. [51] proposed the use of FPGAs to accommodate spiking neurons and unsupervised spike-time dependent plasticity (STDP) learning structures. In this work, Cassidy et al. [51] demonstrated that digital neuron abstraction is preferable to more realistic analogue neurons; they also emulated the massive parallelism connectivity and high neuron density as observed in nature; the neuron states were also multiplexed to take advantage of clock frequencies and dense SRAMs.

Moeys et al. [52] implemented object motion cells in FPGAs that takes about 22 clock cycles at 50 MHz to detect motion and also reported that the FPGA is at least 100 times less than an Intel Next Unit of Computing (NUC) to compute motion. Furthermore, the work in [52] shows that the FPGA

implementation has lower latency when compared with the same implementation running on Intel NUC at 1.30 GHz and an Intel I7-4770 kHz at 3.50 GHz.

Chen et al. [53] described a Central Pattern Generator (CPG) composed of two reciprocally inhibitory neurons. To reduce the FPGA resources usages, Chen et al. [53] has optimised the CPG to avoid using multipliers (FPGAs have a low quantity of multiplier blocks), and the non-linear parts of the Komendantov-Kononenko neuron model [54] were removed. Cheung et al. [55] proposed the NeuroFlow, a scalable SNN simulator suitable to be implemented on FPGA clusters. It was possible to simulate about 600,000 neurons and to get a real-time performance for up to 400,000 neurons simulated using NeuroFlow on 6 FPGAs [55]. Podobas and Matsuoka [47] proposed the use of OpenCL, an HLS tool, to increase productivity by facilitating the SNN design (provide a higher level of hardware abstraction) on FPGAs. Two different neuron models, their axons and synapses, were designed using OpenCL and Authors claim a speed performance of up to 2.25 GSpike/second. Sakellariou et al. [56] suggested a spiking accelerator base on FPGAs to enable users to develop SNNs targeting ML applications and promise an acceleration of up to 800 times for inference and up to 500 times for training compared to Software SNN simulations.

The OpenCV library [57] is one of the most robust and reliable computer vision libraries that includes BS algorithms the GSOC which is most efficient DBS algorithm designed for modelling the dynamic background changes and classifying all the background outliers as foreground. The GSOC algorithm has demonstrated better accuracy on the CDnet2012 and CDnet2014 datasets [58], [59] when compared to other algorithms available on the OpenCV library. Machado et al. [14] proposed the HSMD model (see Figure 1) inspired by the object motion functionality exhibited by vertebrate retinas, in which Object Motion Sensitive - Ganglion Cells (OMS-GC) determine the difference between a local patch's motion trajectory and the background [9]. The HSMD uses a 3-layer SNN to enhance the GSOC BS algorithm [58], [60], [14].

The works reviewed in this section demonstrated that FPGAs offer flexibility, high efficiency, low-power, and high degree of parallelism, making FPGAs the most suitable devices for implementing brain-like circuits. FPGAs enable the design of complex biological plausible neuron models and massively parallel SNN composed of thousands of LIF neurons capable of generating complex biological like patterns. Although FPGA devices being normally programmed complex Hardware Description Language HDL tools, HLS tools such as OpenCL can be used to increase the productivity of SNNs design process by providing hardware abstraction which reduces the implementation complexity. The NeuroHSMD reported in this paper, improves the speed of the HSMD [14] without degradation of the background subtraction accuracy using an high-end FPGA device.

III. HARDWARE PLATFORM

The HSMD algorithm [14] has proven to be very sensitive to object motion events triggered by objects as a direct con-

sequence of using an SNN to emulate the basic functionality observed in OMS-GC. The SNN utilised is composed of 4 layers of neurons interconnected on a 1:1 synaptic connectivity. SNNs are, by their parallel nature, not optimised for sequential processing architectures such as CPU architectures. FPGAs were the obvious choice for accelerating the SNN in the HSMD algorithm because they offer the flexibility to describe massively parallel architectures.

FPGAs are typically reprogrammed using VHDL or Verilog, which are flexible but complex HDLs. In recent years, the FPGA manufacturers have invested in HLS tools to enable Users to program FPGAs using C-like programming languages. One of the most successful HLS tools is OpenCL, which allows users to program kernels that can be compiled targeting CPUs, GPUs, and FPGAs. The NeuroHSMD presented in this paper was implemented using OpenCL on FPGAs.

The SNNs are composed of a variable number of spiking neurons, and each neuron output will contribute to the generation of spike events. Spiking neuron models are therefore highly parallelisable and not computationally suitable for CPUs.

A. Heterogeneous Computing Platforms

The rise of AI and the continuous generation of Big Data are creating computational challenges. CPUs are not enough to efficiently run state-of-the-art AI algorithms or process all the data generated by a wide range of sensors. World-leading processing technology companies (such as NVIDIA, AMD, Intel, ARM and Xilinx) have been looking closely into the new requirements. They have been pushing the boundaries of technology for delivering efficient and flexible processing solutions.

Heterogeneous computing refers to the use of different types of processor systems in a given scientific computing challenge. Heterogeneous platforms are composed of different types of computational units and technologies. Such media can be composed of multi-core CPUs, GPUs and FPGAs acting as computational units and offering flexibility and adaptability demanded by a wide range of application domains [61]. These computational units can significantly increase the overall system performance and reduce power consumption by parallelising concurrent operations that require substantial CPU resources over long periods.

Accelerators like GPUs and FPGAs are massive parallel processing systems that enable accelerating portions of code that are parallelisable. Combining CPUs with GPUs and FPGAs helps improve the performance by assigning different computational tasks to specialised processing systems. GPUs are optimised to perform matrix multiplications in parallel, which is the major bottleneck in video processing and computer graphics. Nevertheless, GPUs also introduce hardware and environmental limitations (e.g. high-power consumption and architectural limitations) [5]. SNNs are massively parallel in their nature and not suitable for matrix representation because each neuron can be considered a node containing several sequential mathematics operations. FPGA devices were

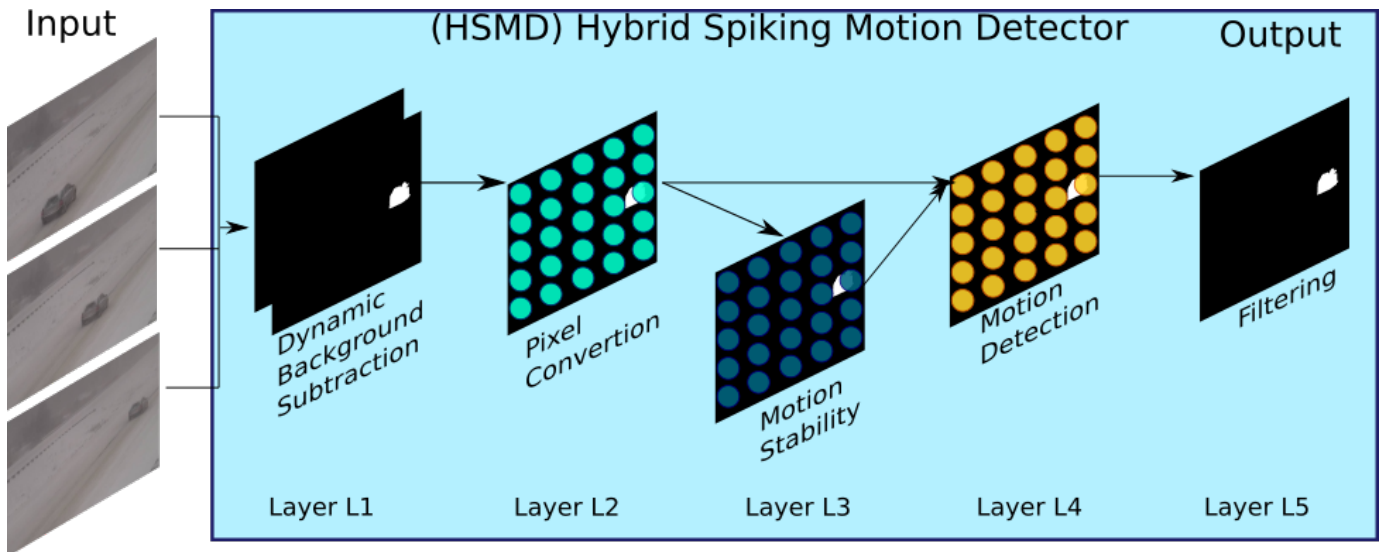


Fig. 1: HSMD architecture implemented by Machado et al. [14]. Composed of 5 layers responsible for 1) performing the dynamic background subtraction, 2) pixel values conversion into currents, 3) motion stability, 4) motion detection, and 5) filtering.

selected to accelerate the SNN, in the HSMD algorithm [14], because of the unique characteristics offered by FPGAs, which enable to accelerate the HSMD's SNN.

OpenCL is a C/C++-based programming language specially designed for Software Developers to write applications targeting heterogeneous computing platforms such as CPUs, GPUs, and FPGAs [62]. OpenCL provides an abstraction layer allowing compatibility across devices and enabling the same source code to run in different device architecture. Furthermore, OpenCL provides facilities for developers to control parallelism and make effective use of the target device resources [63]. OpenCL was the selected framework to ensure that the NeuroHSMD is widely compatible with a wide range of hardware devices for further details about OpenCL).

B. Field Programmable Gate Arrays (FPGA)

FPGAs have been used, for many decades, accelerating applications, including edge/cloud computing. FPGAs are flexible devices because of their flexible architecture enables developers to describe customised architectures. Such flexibility comes with a downside because FPGAs are also known by their associated complexity. There are two main FPGA manufacturers, namely, Intel¹ and Xilinx². The target board is fitted with a state-of-the-art Stratix 10 SoC FPGA device³. Therefore, this section will be focused on the Intel Stratix architecture.

The Intel Stratix family is composed of logic array blocks (LAB) made of 10 basic building blocks called adaptive logic modules (ALMs). Each ALM is composed of fractionable

Look-Up-Tables, also known as adaptive LUT (ALUT), two-bit full adder and four registers.

LABs can be freely reconfigured to implement logic and arithmetic functions. Furthermore, up to a quarter of the LABs can be used as memory LABs (MLABs). Each LAB contains dedicated logic elements used to driving control signals to ALMs. Each MLAB supports up to 640 bits of simple dual-port SRAM. It is possible to configure each ALM in an MLAB as 32×2 memory blocks equivalent to $32 \times 2 \times 10$ simple dual-port SRAM blocks. Dual-port SRAMs are low-latency memory devices that only takes a clock cycle to perform a read/write operation (for example, SDRAM in CPUs takes thousands of clock cycles to complete read/write operations).

C. Hardware Description Languages (HDL)

The behaviour of LABs and ALMs can be programmed using HDL. Although many HDLs being available, the IEEE endorses the VHDL and Verilog. Although the VHDL syntax is identical to Pascal and the Verilog syntax is identical to C, both languages are easy to learn and hard to master. HDLs are potent tools because they enable users to program at the Registers Transfer Level (RTL) (lowest level of coding) which is challenging to master. Hardware developers must have a deep knowledge of the reprogrammed device. Projects designed for a specific FPGA device might not work in another, even if they belong to the same FPGA family. Furthermore, the debugging of HDL source code is very slow and prone to errors, making applications a long and time-consuming process due to complex FPGA architecture.

The FPGA manufacturers have been simplifying the FPGA design flow through the High Level of Synthesis (HLS). HLS tools deliver C/C++ like tools providing higher-level hardware abstraction enabling Software Developers to use FPGAs.

¹Available online, <https://www.intel.co.uk/content/www/uk/en/products/programmable/fpga.html>, last accessed: 04/03/2021

²Available online, <https://www.xilinx.com/>, last accessed: 04/03/2021

³Available online, <https://www.intel.co.uk/content/www/uk/en/products/programmable/soc/stratix-10.html>, last accessed: 07/04/2021

D. Open Computer Language (OpenCL)

OpenCL applications are split into two parts, namely, **host** application(s) and **device** kernel(s). The **host** application(s) is(are) always compiled on the host Operating System and runs on a CPU. **Host** applications are also used to launch the target kernels on the target **devices**. Kernels are special functions written in OpenCL C/C++ to perform parallelisable computations on accelerators such as GPUs and FPGAs [63]. For instance, consider two $m \times n$ matrices A and B where it is expected to do the operation $C=A+B$ where C is the third matrix of $m \times n$. In this case, the kernel could just perform, in parallel, the addition of matrices A and B elements and store the result in C. Unlike in CPUs, where it would take $m \times n$ to do this matrix addition, GPUs and FPGAs could parallelise this operation depending on the resources available per device resulting in the acceleration of the application. Buffer objects within a context are used in OpenCL to exchange data between the host and device [64]. The Intel FPGA Software Development Kit (SDK) for OpenCL offline compiler optimises the kernel throughput by adjusting buffer sizes during the kernel compilation process [65]. OpenCL provides both mapped and asynchronous buffers enabling the application to continue to run while additional data is exchanged.

Software Developers have to carefully analyse the code to be optimised and only select the sections that may benefit the hardware acceleration because the maximum speed is always dictated by the PCIe BUS speed. Another big challenge for Software Developers is the low debugging capabilities available while the code is being executed on the device.

Although it is possible to use OpenCL to program FPGA and GPU devices, GPUs are specialised devices designed for video rendering and graphics processing. At the same time, FPGAs are customisable devices that can be freely reconfigurable. Therefore, FPGAs offer more flexibility than GPUs, which is desirable for accelerating SNNs because they can be modelled using the Network-on-Chip NoCs concept. Each individual spiking neuron in the node interconnects to one or more nodes of the same SNN. The flexibility offered by both FPGAs and OpenCL makes the selection of FPGAs over GPUs the obvious choice.

Intel FPGA SDK for OpenCL (IOCL) provides a compiler and powerful tools to build and run OpenCL applications targeting Intel FPGA devices. The IOCL generates two main components: the host application and the FPGA programming bitstream(s). The IOCL offline compiler (AOC) first compiles the custom kernel(s) to an image file (*.aocx) that will be used to program the FPGA. In contrast, the host-side C/C++ compiler compiles the host application and then links it to the IOCL runtime libraries.

The IOCL compiles one or more OpenCL kernels and creates a hardware configuration file. A successful compilation results in a *.aocr, *.aoco, *.aocx and reports/report.html files. The report.html contains the estimated resource usage and a preliminary assessment of area usage. The intermediary *.aoco and *.aocr are only used in the generation of the *.aocx which is then used to program the FPGA.

Although there are hundreds of FPGA boards, only a few

boards provide board support packages (BSP) for OpenCL. The creation of the OpenCL BSP for a given FPGA is a complex and time-consuming process that considers the FPGA device and how the Inputs/Outputs are routed in the physical board. Therefore, the selection of the FPGA board should be made taking into consideration the size of the FPGA device, the OpenCL BSP, the version of the BSP to ensure compatibility with recent Linux distributions and the reference/user manuals.

The Terasic DE10-pro development board [66] was used for implementing the NeuroHSMD discussed in this section. The Terasic DE10-pro development board is equipped with a state-of-the-art high-end Intel Stratix 10 FPGA device. Terasic states that DE10 pro was designed to fulfil the demands of AI, Data Center, and High-Performance Computing. Furthermore, the DE10-pro development board takes advantage of the latest Intel Stratix 10 to obtain high-speed and low-power (with up to 70% lower power). It is equipped with 32GB DDR4 memory module running at over 150 Gbps, up to 15.754 GB/s data transfer via PCIe Gen 3 x16 edge between FPGA and host PC, and 4 onboard QSFP28 (100GbE) connectors. The DE10 pro was installed on the host PC equipped with an Intel(R) Core(TM) i7-4770 CPU @ 3.40GHz and 16 GB of DDR3 using the PCIe slot.

IV. NEUROHSMD ARCHITECTURE

The NeuroHSMD architecture is described in this section. As mentioned above, OpenCL was used to implement SNN on the FPGA device. In OpenCL, the data exchanged between the host application and the FPGA kernels flow is as follows: a) allocation and specification of buffer type (i.e. read or write) on the host and device; b) copy data from the application data structures to host buffers; c) transfer data from host buffers to device buffers; d) run the inference on the device; e) copy the results from device to host buffers; f) copy data from the host buffers to application data structures (see Figure 2).

The NeuroHSMD algorithm performs the following stages of computation: 1) image capture, 2) conversion from colour to grey, and 3) dynamic background subtraction using the OpenCL's GSOC algorithm and copy resulting pixel values are buffered and transferred to the FPGA device; 4) run the inference on the FPGA and wait for the spike results; 5) run the SNN kernel, 6) Filtering using an average filter, and 7) Display and save the output image. The NeuroHSMD computation stages are summarised in diagram 3 and the NeuronHSMD architecture is depicted in Figure 4.

Furthermore, the NeuronHSMD OpenCL is composed of the NeuroHSMD Host Application (NHA) and the NeuronHSMD Device Kernel (NHK). Details about the NHA and NDK are given in sections IV-1 and IV-2.

1) *Host application*: The NeuronHSMD Host Application (NHA) is used to interface the two NeuronHSMD device kernels (NDKs). The NHA performs the first stages of pre-processing and performs inference of the SNN kernel (described on the FPGA), and uses the inference results to compute the BS. Furthermore, the NHA can process both

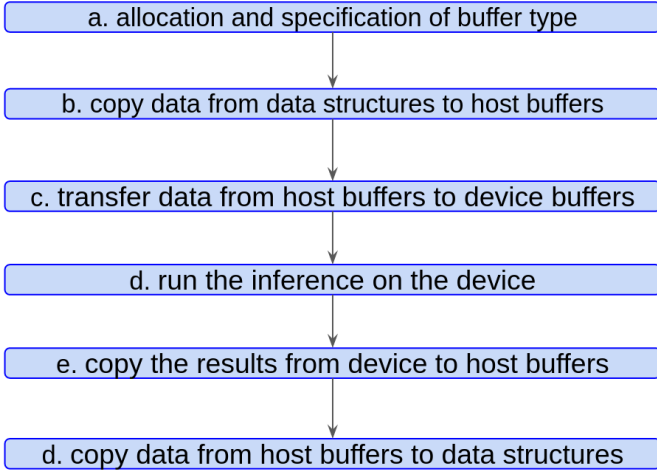


Fig. 2: OpenCL stages. The stages include: a) allocation and specification of buffer type on the host and device; b) copy data from the application data structures to host buffers; c) transfer data from host buffers to device buffers; d) run the inference on the device; e) copy the results from device to host buffers; f) copy data from the host buffers to application data structures.

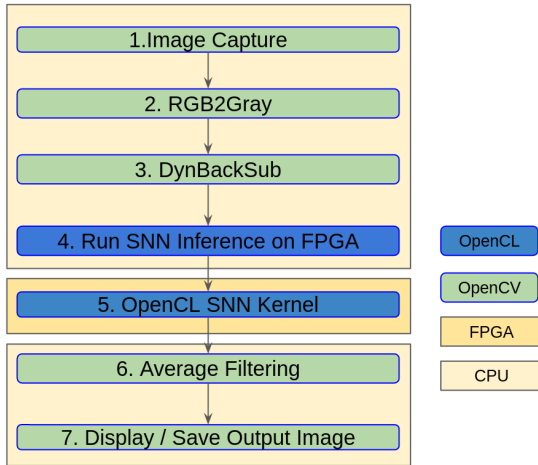


Fig. 3: NeuroHSMD computation stages. The OpenCL implementation is represented in blue and the OpenCV in green. The light yellow background represents the computation stages that run on the CPU (i.e. 1, to 4 and 6 to 7), and in light orange the stage that runs on the FPGA device (i.e. 5).

live images captured from camera devices or extracted from videos stored on USB or SATA devices. The NHA is used to interface the two NeuroHSMD device kernels. The NHA performs the first stages of pre-processing and performs inference of the NDK (described on the FPGA), and uses the inference results to compute the BS. Furthermore, the NHA can process both live images captured from camera devices or extracted from videos stored on USB or SATA devices.

Algorithm 1 summarises each of the computation stages that occur in the NHA. The communication between the NHA and

the NDK is limited by the PCIe BUS speed (16 GB/s⁴). In the HSMD, the limitations are only dictated by the CPU speed and the DDR4 memory speed (34.1 GB/s⁵) which 2x faster than the PCIe BUS speed.

2) *Device kernels*: The NDKs section covers the two kernels (i.e. NeuroHSMDv1 and NeuroHSMDv2) that have been implemented. The difference NDKs is that *aocl_snn_v1* computes the spike sum for all the neurons, and *aocl_snn_v2* only computes the spike sums for neurons that have the pixel intensity values greater than 0.0.

Fig. ?? depicts the seven stages of computation and exhibits the place where each stage occurs (i.e. CPU or FPGA). Both, NeuroHSMDv1 and NeuroHSMDv2 NDKs implement the HSMD's SNN (see Figure 5).

The *aocl_snn_v1* was parallelised by factor of 16. The NDK version 1 is the equivalent implementation of the HSMD algorithm [14] which is called HSMDv1 in this section.

The Algorithm 3, inferred by the NHP, summarises the computation steps required compute the spikes sum.

Fig. ?? depicts the seven stages of computation and exhibits the place where each stage occurs (i.e. CPU or FPGA).

The *aocl_snn_v2* was parallelised by factor of 16. The NDK version 1 contains an optimisation where the spike sum for a given neuron of layer 1 is only computed if the pixel intensity value is greater than 0.0. This optimisation was also applied to the original HSMD Algorithm [14]. The optimised version of the HSMD is called HSMDv2 in this section.

A. Datasets and Benchmark

The NeuroHSMDv1, NeuroHSMDv2, HSMDv1 and HSMDv2 were tested against the CDnet2012 [15] and CDnet2014 [16] and compared the original scripts provided by Nil Goyette et al. [15] following the same protocol used to test the HSMD algorithm [14]. The scripts provided by Nil Goyette et al. [15] enables the computation of eight metrics.

The average performance obtained for each category using each BS method and the HSMD and NeuroHSMD algorithms are characterised via eight metrics, as shown below. The four base qualitative metrics are: True Positive (TP), True Negative (TN), False Positive (FP) and False Negative (FN) [15], [16].

- 1) Recall (Re): $Re = \frac{TP}{TP+FN}$
Re: ranked by **descending order**;
- 2) Specificity (Sp): $Sp = \frac{TN}{TN+FP}$;
Sp ranked by **descending order**;
- 3) False Positive Rate (FPR): $FPR = \frac{FP}{FP+TN}$;
FPR ranked by **ascending order**;
- 4) False Negative Rate (FNR): $FNR = \frac{FN}{FN+TP}$;
FNR ranked by **ascending order**;
- 5) Wrong Classification Rate (WCR): $WCR = \frac{FN+FP}{TP+FN+FP+TN}$;
WCR ranked by **ascending order**;
- 6) Correct Classification Rate (CCR): $CCR = \frac{TP+TN}{TP+FN+FP+TN}$;

⁴Available online, <https://www.trentonsystems.com/blog/pcie-gen4-vs-gen3-slots-speeds>, last accessed: 21/06/2021

⁵Available online, <https://www.crucial.com/support/articles-faq-memory/understanding-cpu-limitations-with-memory>, last accessed: 21/06/2021

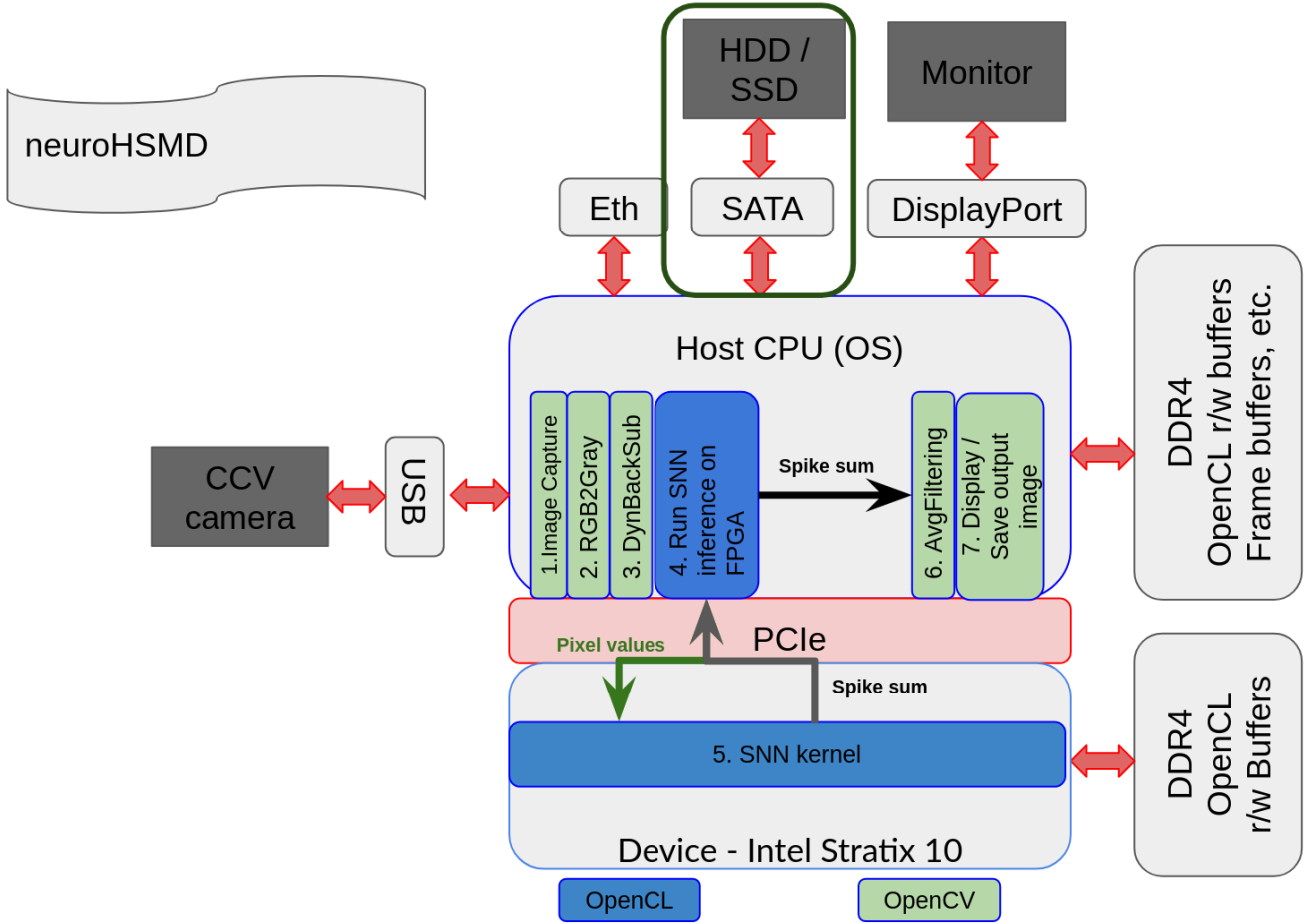


Fig. 4: NeuroHSMD architecture. The diagram represents the computation stages that run both on the CPU and FPGA. Shows that the FPGA is connected to the host CPU via the PCI express bus. It also shows the dedicated memory of the CPU and FPGA device. Includes also how external devices (e.g. CCV, monitor and HDD/SSD) connect to the host CPU via different interfaces (e.g. ethernet (eth), sata, display port and usb). The computations stages implemented in OpenCL are in blue and OpenCV in green.

5. SNN kernel

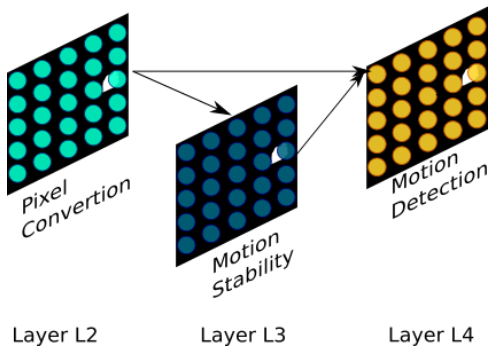


Fig. 5: NDKs implementation. The HSMD's SNN includes: Layer L2 - conversion of pixel values to currents, Layer L3 - motion stability and Layer L4 - motion detection

CCR ranked by **descending order**;

7) Precision Pr: $Pr = \frac{TP}{TP+FP}$;

Pr ranked by **descending order**;

8) F1-Score (F1): $F1 = 2 \times \frac{Pr \cdot Re}{Pr + Re}$

$F1$ ranked by **descending order**;

$$\frac{\text{Average Ranking (R)}}{\overline{Re+Sp+FP+FN+WC+CCR+F1}}; \quad R =$$

R ranked by **ascending order**;

$$\overline{RC} = \frac{\text{Average Ranking across all categories (RC)}}{\overline{Re+Sp+FP+FN+WC+CCR+F1}};$$

\overline{RC} ranked by **ascending order**;

where $nMet$ is the number of metrics (8 in this case).

The benchmark of the four algorithms is required to ensure that the four algorithms produce comparative results to that of the original HSMDv1 results when tested against CDnet2012 and CDnet2014 datasets. Furthermore, the OpenCL calls the Intel Quartus, which performs several hardware optimisations that may include converting from floating-point to fixed-point representation, which might affect the accuracy of the NeuroHSMD algorithms during the synthesis step (one of the steps of the OpenCL design flow).

Algorithm 1 NeuroHSMD hardware application.

Input:

img: image frame;

Output:

post_proc_img: post processed image;

stats: computation statistics;

Main Algorithm:

```

1: initialise_opencl()
2: for iterator ← list_folders.begin() to list_folders.end() do
3:   (x,y) ← get_image_size();
4:   num_layers ← 3
5:   tot_neurons ← x.y.num_layers
6:   reset_opencl_buffers(tot_neurons )
7:   gsoc ← initialise_gsoc_back_subtraction
8:   for iterator2 ← files_list.begin() to files_list.end() do
9:     img ← read_image(iterator2);
10:    < pixel_values > ← gsoc.compute(img)
11:    aocl_snn_v1(< pixel_values >) → < spike_sum > {Alg. 2}
12:    OR
13:    aocl_snn_v2(< pixel_values >) → < spike_sum > {Alg. 3}
14:    post_proc_img ← get_spikes_sum_l3(< spike_sum >)
15:    save(post_proc_img)
16:    stats ← compute_stats(time)
17:  end for
18:  save(stats)
19: end for

```

V. RESULTS

The HSMDv1, HSMDv2, NeuroHSMDv1 and NeuroHSMDv2 where all tested on the same computer equipped with a quad-core Intel(R) Core(TM) i7-4770 CPU @ 3.40GHz, 16GB of DDR3 @ 1600 MHz and 1TB of HDD. The

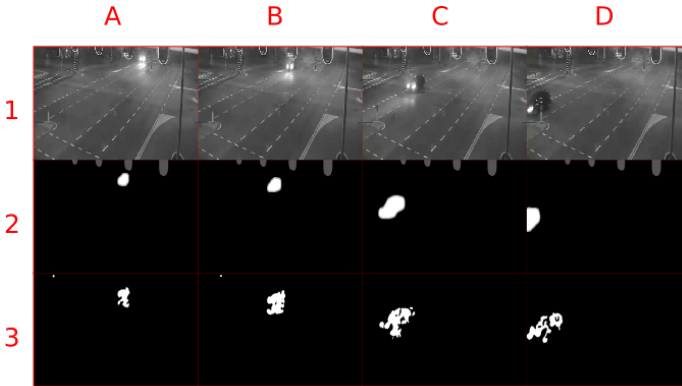


Fig. 6: Example of the processed images. Row 1: input image sequences, Row 2: ground truth for each input images and Row 3: NeuroHSMDv1 output.

The results section is divided into three parts. Namely, Section V-A shows the resources usage to enable the comparison between the two kernels' complexity, the speed performance results are presented in Section V-B and Section V-C shows

the benchmark results when tested against the CDnet2012 and CDnet2014 datasets.

A. Resources Usage

The resources usage are given the report generated by the *aoc* after the successful completion of the kernel compilation, which can take several hours (typically between 6h and 24h depending on the kernel complexity for the DE10pro). The resources usage for the compilation of the NeuroHSMDv1 kernels is given in Table I and the NeuroHSMDv2 kernel in Table II.

From the analysis of Table I can be seen that the estimated resource utilisation is more pessimist than the final resource utilisation, which is a direct consequence of the Intel Quartus's optimisations during the synthesis and routing phases and to ensure that circuit fits in the FPGA device. Nevertheless, it takes about 5 minutes to get the *estimated resources usage* and between 6h to 24h to get the *resources utilisation summary*. Therefore, it is a good practice defining the coefficient **N** in the statement **# PRAGMA UNROLL N** based on the *estimated resources usage*.

Again, from the analysis of Table II it can be seen that the estimated resource utilisation is higher than the actual resource utilisation as a consequence of the Intel Quartus's optimisations during the synthesis and routing phases.

The NDK v2 compared with the NDK v1, consumes 1448.7 ALMs less, 25423 FFs less, 2 RAMs less and the same number of DSPs. Nevertheless, the NDK v2 kernel max frequency is 300MHz, while the NDK v1 kernel max frequency is 306.25

Algorithm 2 aocl_snn_v1**Parallel Circuits:** 16**Constants:**

R_m : membrane resistance;
 τ_m : membrane time constant;
 dt : time step;
 $p2c$: pixel values to current;
 $steps$: number of steps;
 $s2c$: spike to current;

Input:

$\langle pixel_val \rangle$: pixel values;
 num_neuron_layer : number of neurons per layer;

Output:

$\langle spk_sum \rangle$: spike sum;

Main Algorithm:

```

1: for neuron_idx ← 0 to number_neurons do
2:    $I_s \leftarrow pixel\_val[neuron\_idx].p2c$ ;
3:   for dt1 ← 0 to steps do
4:     Layer 1:
5:      $compute\_V_m\_l1[neuron\_idx](I_s)$ ;
6:      $update\_spike\_sum\_l1[neuron\_idx](V_m\_l1)$ ;
7:     Layer 2:
8:      $I_s\_l2 \leftarrow spike\_sum\_l1[neuron\_idx].s2c$ ;
9:      $compute\_V_m\_l2[neuron\_idx](I_s\_l2)$ ;
10:     $update\_spike\_sum\_l2[neuron\_idx](V_m\_l2)$ ;
11:    Layer 3:
12:     $I_s\_l3 \leftarrow spike\_sum\_l2[neuron\_idx].s2c$ ;
13:     $compute\_V_m\_l3[neuron\_idx](I_s\_l2 + I_s\_l3)$ ;
14:     $update\_spk\_sum[neuron\_idx](V_m\_l3)$ ;
15:   end for
16: end for

```

MHz. The NDK v2 enables saving of less than 1% of resources and introduces a 2% increase in latency.

The coefficient N should always be a multiple of 2^n to ensure the optimal use of FPGA resources. For example, the resources usage of $N = 48$ is equivalent to $N = 64$. Moreover, both NDKs had failed to compile when $N = 32$ because there was not enough ALUTs. The design required more ALUTs than those available on the device, violating the compilation rules because the design would not fit on the device.

B. Speed Performance

The speed results obtained for the four algorithms tested against the CDnet2012 shown in Table III.

From Table III can be seen that both the NeuroHSMDv1 and NeuroHSMDv2 have performed better than the software versions (i.e. HSMDv1 and HSMDv2). It is also apparent that the NeuroHSMDv1 performs better in images with higher resolution (i.e. 720×480 and 720×576) while the NeuroHSMDv2 in lower resolutions (i.e below 720×480). Overall, the NeuroHSMDv2 had an average frame rate of 71.50 fps, NeuroHSMDv1 63.20 fps, HSMDv2 40.26 fps, HSMDv1 36.11 fps. Finally, the average frame rate for processing images with the native resolution of 720×480 per algorithm is i) NeuroHSMDv1 28.06 fps, NeuroHSMDv2 25.45 fps, HSMDv2 11.19 fps and HSMDv1 9.97 fps.

The speed results obtained for the four algorithms when tested against the CDnet2014 are depicted in Table IV.

Table IV shows that the NeuroHSMDv1 and NeuroHSMDv2 have performed better than the software versions (i.e. HSMDv1 and HSMDv2) when tested against the CDnet2014 dataset. Once again, the NeuroHSMDv1 performs better in images with higher resolution (i.e. equal or higher than 480×295) while the NeuroHSMDv2 in lower resolutions (i.e below 480×295). Overall, the NeuroHSMDv2 has an average frame rate of 43.51 fps, NeuroHSMDv1 39.94 fps, HSMDv1 29.30 fps, and HSMDv2 25.18 fps. It is essential to highlight that the CDnet2014 has more categories and image sequences, leading to different frame rates for the CDnet2012 and CDnet2014 datasets.

The average frame rate for processing images with the native resolution of 720×480 per algorithm was i) NeuroHSMDv1 28.71 fps, NeuroHSMDv2 24.95 fps, HSMDv2 12.37 fps and HSMDv1 11.25 fps. These results are in line with the results obtained for the 4 algorithms when tested against the CDnet2012 dataset.

C. Benchmark

Table V shows the results obtained after testing the 4 methods against the CDnet2012 ground-truth images using the scripts provided by Nil Goyette et al. [15].

Algorithm 3 aocl_snn_v2**Parallel Circuits:** 16**Constants:**

R_m : membrane resistance;
 τ_m : membrane time constant;
 dt : time step;
 $p2c$: pixel values to current;
 $steps$: number of steps;
 $s2c$: spike to current;

Input:

$\langle pixel_val \rangle$: pixel values;
 num_neuron_layer : number of neurons per layer;

Output:

$\langle spk_sum \rangle$: spike sum;

Main Algorithm:

```

1: for neuron_idx ← 0 to number_neurons do
2:   if pixel_val[neuron_idx] > 0.0 then
3:      $I_s \leftarrow pixel\_val[neuron\_idx].p2c$ ;
4:     for dt1 ← 0 to steps do
5:       Layer 1:
6:          $compute\_V_m\_l1[neuron\_idx](I_s)$ ;
7:          $update\_spike\_sum\_l1[neuron\_idx](V_m\_l1)$ ;
8:       Layer 2:
9:          $I_s\_l2 \leftarrow spike\_sum\_l1[[neuron\_idx].s2c$ ;
10:         $compute\_V_m\_l2[[neuron\_idx](I_s\_l2)$ ;
11:         $update\_spike\_sum\_l2[neuron\_idx](V_m\_l2)$ ;
12:      Layer 3:
13:         $I_s\_l3 \leftarrow spike\_sum\_l2[neuron\_idx].s2c$ ;
14:         $compute\_V_m\_l3[neuron\_idx](I_s\_l2 + I_s\_l3)$ ;
15:         $update\_spk\_sum[neuron\_idx](V_m\_l3)$ ;
16:      end for
17:    end if
18:  end for

```

From the results shown in Table V it is possible to infer that the results obtained with the four methods are equivalent because all the methods were ranked in first place with the same values per metrics. Indexing all the algorithms in the first place was expected because the speed optimisation in version 2 of the NeuroHSMD and HSMD should not interfere with the model dynamics.

Table VI depicts the results obtained after testing 4 methods against the CDnet2014 ground-truth images using the scripts provided by Nil Goyette et al. [15].

From the results shown in Table VI it is possible to infer that the results obtained with the four methods are probably the same because the four methods were ranked, again, in first place with the same values per metrics. These results were important because it is possible to infer that there has no degradation of the accuracy as consequence of the hardware acceleration.

VI. CONCLUSIONS AND FUTURE WORK

Two bio-inspired NeuroHSMD have been proposed to accelerate the HSMD algorithm [14]. The NeuroHSMDv1 and NeuroHSMDv2 (speed optimisation) were tested against the CDnet2012 and CDnet2014 datasets. The NeuroHSMDv1

has lower latency when processing images with resolutions equal to or greater than 480×295 . The NeuroHSMDv2 (speed optimisation) has a lower latency when processing images with resolutions smaller than 480×295 . Two HSMD versions were used (the original HSMDv1 algorithm [14] and HSMDv2 with speed optimisation) for ensuring a fair comparison between the software and hardware implementations. The HSMDv1, HSMDv2, NeuroHSMDv1 and NeuroHSMDv2 were all tested on the same computer equipped with a quad-core Intel(R) Core(TM) i7-4770 CPU @ 3.40GHz, 16GB of DDR3 @ 1600 MHz and 1TB of HDD. The average frame rate for processing images with the native resolution of 720×480 per algorithm was

CDnet2012:

i) NeuroHSMDv1 28.06 fps, NeuroHSMDv2 25.45 fps, HSMDv2 11.19 fps and HSMDv1 9.97 fps

CDnet2014:

i) NeuroHSMDv1 28.71 fps, NeuroHSMDv2 24.95 fps, HSMDv2 12.37 fps and HSMDv1 11.25 fps.

The four methods were also tested against the ground-truth images available in the CDnet2012 and CDnet2014 datasets using the eight metrics, were used to assess and compare the quality of the HSMD algorithm. The four methods obtained

TABLE I NeuroHSMDv1 resources usage.

| <i>Summary</i> | | | | | |
|---|--|--------------|----------------|-----------------|-----------------------------|
| Info | | | | | |
| Project Name | snn_pc_v1 | | | | |
| Target Family, Device, Board | Stratix 10, 1SG280LU3F50E1VGS1, de10_pro:s10_sh2e1_4Gx2 | | | | |
| AOC Version | 19.1.0 Build 240 | | | | |
| Quartus Version | 19.1.0 Build 240 Pro | | | | |
| Command | aoc device/snn_pci_v1.cl -o bin_acl/snn_pci_v1.aocx -v -report -board=s10_sh2e1_4Gx2 -incremental | | | | |
| Quartus Fit Clock Summary | | | | | |
| Frequency (MHz) | 306.25 (fmax) | | | | |
| Quartus Fit Resource Utilisation Summary | | | | | |
| | <i>ALMs</i> | <i>FFs</i> | <i>RAMs</i> | <i>DSPs</i> | <i>MLABs</i> |
| Full design (all kernels) | 387168.7 | 985558 | 2231 | 1408 | 4766 |
| snn | 488257.1 | 1060084 | 2484 | 1024 | 3871 |
| Kernel Summary | | | | | |
| Kernel Name | Kernel Type | Autorun | Workgroup Size | # Compute Units | Hyper-Optimised Handshaking |
| snn | 488257.1 | 1060084 | 2484 | 1024 | 3871 |
| Estimated Resource Usage | | | | | |
| Kernel Name | ALUTs | FFs | RAMs | DSPs | MLABs |
| snn | 488257.1 | 1060084 | 2484 | 1024 | 3871 |
| Global Interconnect | 10629 | 16485 | 61 | 0 | 0 |
| Board Interface | 13132 | 20030 | 112 | 0 | 0 |
| System description ROM | 2 | 71 | 2 | 0 | 0 |
| Total | 567523 (30%) | 907449 (24%) | 2963 (25%) | 976 (17%) | 3786 |
| Available | 1866240 | 3732480 | 11721 | 5760 | 0 |
| Compile Warnings | | | | | |
| None | | | | | |

the same values for all the metrics and were all ranked first. The first place acquired by the four methods is an indication that there was no degradation with the hardware acceleration. Future work includes optimising the HSMD algorithm to detect and track motion in challenging scenarios (e.g. low frame rate, dynamic background and camera jitter) and an investigation to verify if the SNN improves the remaining methods' output. It is also planned the implementation and evaluation of more complex retinal cells (such as predictive cells) using SNNs and assess for optimising BS algorithms and accelerate such complex retinal cells using FPGA technology.

REFERENCES

- [1] L. A. Pastur-Romay, A. B. Porto-Pazos, F. Cedron, and A. Pazos, "Parallel Computing for Brain Simulation," *Current Topics in Medicinal Chemistry*, vol. 17, pp. 1646–1668, apr 2017.
- [2] R. Brooks, D. Hassabis, D. Bray, and A. Shashua, "Is the brain a good model for machine intelligence?," *Nature*, vol. 482, pp. 462–463, feb 2012.
- [3] S. Herculano-Houzel, "The human brain in numbers: a linearly scaled-up primate brain," *Frontiers in Human Neuroscience*, vol. 3, nov 2009.
- [4] P. J. Fox, "Massively Parallel Neural Computation," *University of Cambridge Computer Laboratory*, no. 830, pp. 1–105, 2013.
- [5] Intel, "What Is a GPU? Graphics Processing Units Defined," 2020.
- [6] Intel, "FPGA vs. GPU for Deep Learning Applications – Intel," 2020.
- [7] M.-N. Chapel and T. Bouwmans, "Moving Objects Detection with a Moving Camera: A Comprehensive Review," jan 2020.
- [8] H. Kolb, "How the Retina Works," *American Scientist*, vol. 91, pp. 28 – 34, 2003.
- [9] T. Gollisch and M. Meister, "Eye Smarter than Scientists Believed: Neural Computations in Circuits of the Retina," *Neuron*, vol. 65, no. 2, pp. 150–164, 2010.
- [10] M. ZHANG, G. Zonghua, and P. Gang, "A survey of neuromorphic computing based on spiking neural networks," *Chinese Journal of Electronics*, vol. 27, no. 4, pp. 667–674, 2018.
- [11] M. Bouvier, A. Valentian, T. Mesquida, F. Rummens, M. Reyboz, E. Vianello, and E. Beigne, "Spiking Neural Networks Hardware Implementations and Challenges," *ACM Journal on Emerging Technologies in Computing Systems*, vol. 15, pp. 1–35, jun 2019.
- [12] J. Von Neumann, "First draft of a report on the edvac," *Moore School, University of Pennsylvania*, 1945.
- [13] S. Blank, "What the GlobalFoundries' Retreat Really Means - IEEE Spectrum," 2018.
- [14] P. Machado, A. Oikonomou, J. F. Ferreira, and T. M. McGinnity, "Hsmd: An object motion detection algorithm using a hybrid spiking neural network architecture," *IEEE Access*, pp. 1–1, 2021. <https://doi.org/10.1109/ACCESS.2021.3111005>.
- [15] N. Goyette, P. M. Jodoin, F. Porikli, J. Konrad, and P. Ishwar, "changedetection.net: A new change detection benchmark dataset," *IEEE Computer Society Conference on Computer Vision and Pattern Recognition Workshops*, pp. 1–8, 2012.
- [16] Y. Wang, P.-M. Jodoin, F. Porikli, J. Konrad, Y. Benezeth, and P. Ishwar, "CDnet 2014: An Expanded Change Detection Benchmark Dataset," in

TABLE II NeuroHSMDv2 resources usage.

| <i>Summary</i> | | | | | |
|---|--|--------------|----------------|-----------------|-----------------------------|
| Info | | | | | |
| Project Name | snn_pci_v2 | | | | |
| Target Family, Device, Board | Stratix 10, 1SG280LU3F50E1VGS1, de10_pro:s10_sh2e1_4Gx2 | | | | |
| AOC Version | 19.1.0 Build 240 | | | | |
| Quartus Version | 19.1.0 Build 240 Pro | | | | |
| Command | aoc device/snn_pci_v2.cl -o bin_acl/snn_pci_v2.aocx -board=s10_sh2e1_4Gx2 -v -report -incremental | | | | |
| Quartus Fit Clock Summary | | | | | |
| Frequency (MHz) | 300 (Kernel fmax) | | | | |
| Quartus Fit Resource Utilisation Summary | | | | | |
| | ALMs | FFs | RAMs | DSPs | MLABs |
| snn | 486808.4 | 1034661 | 2486 | 1024 | 3933 |
| Kernel Summary | | | | | |
| Kernel Name | Kernel Type | Autorun | Workgroup Size | # Compute Units | Hyper-Optimised Handshaking |
| snn | Single work-item | No | 1,1,1 | 1 | Off |
| Estimated Resource Usage | | | | | |
| Kernel Name | ALUTs | FFs | RAMs | DSPs | MLABs |
| snn | 530436 | 844793 | 2868 | 976 | 3844 |
| Global Interconnect | 10629 | 16485 | 61 | 0 | 0 |
| Board Interface | 13132 | 20030 | 112 | 0 | 0 |
| System description ROM | 2 | 71 | 2 | 0 | 0 |
| Total | 554199 (30%) | 881379 (24%) | 3043 (26%) | 976 (17%) | 3844 |
| Available | 1866240 | 3732480 | 11721 | 5760 | 0 |
| Compile Warnings | | | | | |
| None | | | | | |

2014 *IEEE Conference on Computer Vision and Pattern Recognition Workshops*, pp. 393–400, IEEE, jun 2014.

- [17] P. Kumar Bheemavarapu, P. Kumar Tadiparthi, S. Ponnada, K. S. Jhansi, and A. Gottimukkala, “A Comprehensive Review of Moving Object Identification Using Background Subtraction in Dynamic Scenes Sreenu Ponnada A Comprehensive Review of Moving Object Identification Using Background Subtraction in Dynamic Scenes,” tech. rep., 2021.
- [18] B. Garcia-Garcia, T. Bouwmans, and A. J. Rosales Silva, “Background subtraction in real applications: Challenges, current models and future directions,” *Computer Science Review*, vol. 35, p. 100204, feb 2020.
- [19] R. A. Hadi, L. E. George, and M. J. Mohammed, “A computationally economic novel approach for real-time moving multi-vehicle detection and tracking toward efficient traffic surveillance,” *Arabian Journal for Science and Engineering*, vol. 42, no. 2, pp. 817–831, 2017.
- [20] Á. Virginás-Tar, M. Baba, V. Gui, D. Pescaru, and I. Jian, “Vehicle counting and classification for traffic surveillance using wireless video sensor networks,” in *2014 22nd Telecommunications Forum Telfor (TELFOR)*, pp. 1019–1022, IEEE, 2014.
- [21] O. Masoud and N. P. Papanikolopoulos, “A novel method for tracking and counting pedestrians in real-time using a single camera,” *IEEE transactions on vehicular technology*, vol. 50, no. 5, pp. 1267–1278, 2001.
- [22] L. Yi, Y. Ting, and L. Xinqiao, “Analysis and simulation of crowd in airport multiple transport modes,” in *Proceedings of the 2020 International Conference on Aviation Safety and Information Technology*, pp. 36–41, 2020.
- [23] S. Chen, Z. Feng, Q. Lu, B. Mahasseni, T. Fiez, A. Fern, and S. Todorovic, “Play type recognition in real-world football video,” in *IEEE Winter Conference on Applications of Computer Vision*, pp. 652–659, IEEE, 2014.
- [24] L. H. Leong, M. A. Zulkifley, and A. B. Hussain, “Computer vision approach to automatic linesman,” in *2014 IEEE 10th International Colloquium on Signal Processing and its Applications*, pp. 212–215, IEEE, 2014.
- [25] S. Guler and M. K. Farrow, “Abandoned object detection in crowded places,” in *Proc. of PETS*, pp. 18–23, Citeseer, 2006.
- [26] E. Cermeño, A. Pérez, and J. A. Sigüenza, “Intelligent video surveillance beyond robust background modeling,” *Expert Systems with Applications*, vol. 91, pp. 138–149, 2018.
- [27] M. Dotter and J. Harguess, “Automated situational reporting,” in *Geospatial Informatics XI*, vol. 11733, p. 117330G, International Society for Optics and Photonics, 2021.
- [28] K. Ren, G. Bernes, M. Hetta, and J. Karlsson, “Tracking and analysing social interactions in dairy cattle with real-time locating system and machine learning,” *Journal of Systems Architecture*, vol. 116, p. 102139, 2021.
- [29] F. Okura, S. Ikuma, Y. Makihara, D. Muramatsu, K. Nakada, and Y. Yagi, “Rgb-d video-based individual identification of dairy cows using gait and texture analyses,” *Computers and Electronics in Agriculture*, vol. 165, p. 104944, 2019.
- [30] C. Yang and J. Collins, “Improvement of honey bee tracking on 2d video with hough transform and kalman filter,” *Journal of Signal Processing Systems*, vol. 90, no. 12, pp. 1639–1650, 2018.
- [31] M. Wu, X. Cao, and S. Guo, “Accurate detection and tracking of ants in indoor and outdoor environments,” *bioRxiv*, 2020.
- [32] J. Zhao, Z. Gu, M. Shi, H. Lu, J. Li, M. Shen, Z. Ye, and S. Zhu, “Spatial behavioral characteristics and statistics-based kinetic energy modeling in special behaviors detection of a shoal of fish in a recirculating aquaculture system,” *Computers and Electronics in Agriculture*, vol. 127, pp. 271–280, 2016.
- [33] G. de Oliveira Feijó, V. A. Sangalli, I. N. L. da Silva, and M. S. Pinho, “An algorithm to track laboratory zebrafish shoals,” *Computers in biology and medicine*, vol. 96, pp. 79–90, 2018.
- [34] H. Ghaffarian, P. Lemaire, Z. Zhi, L. Tougne, B. MacVicar, and

TABLE III CDnet2012 speed result.

| Category | no. imgs | height | width | NeuroHSMDv1 | | NeuroHSMDv2 | | HSMDv1 | | HSMDv2 | |
|---|----------|--------|-------|-------------|-------|-------------|-------|---------|-------|---------|-------|
| | | | | SNN [s] | FPS | SNN [s] | FPS | SNN [s] | FPS | SNN [s] | FPS |
| baseline/PETS2006 | 1199 | 576 | 720 | 0.0078 | 23.66 | 0.0181 | 20.45 | 0.0274 | 8.40 | 0.0209 | 9.73 |
| cameraJitter/badminton | 1149 | 480 | 720 | 0.0068 | 28.33 | 0.0151 | 25.48 | 0.0214 | 10.01 | 0.0181 | 11.50 |
| dynamicBackground/fall | 3999 | 480 | 720 | 0.0068 | 27.28 | 0.0152 | 25.01 | 0.0200 | 9.87 | 0.0180 | 11.08 |
| shadow/copyMachine | 3399 | 480 | 720 | 0.0067 | 28.56 | 0.0152 | 25.86 | 0.0208 | 10.04 | 0.0183 | 10.98 |
| dynamicBackground/fountain01 | 1183 | 288 | 432 | 0.0034 | 55.17 | 0.0066 | 58.30 | 0.0075 | 27.40 | 0.0062 | 29.99 |
| dynamicBackground/fountain02 | 1498 | 288 | 432 | 0.0034 | 56.12 | 0.0066 | 58.13 | 0.0074 | 27.64 | 0.0061 | 30.37 |
| intermittentObjectMotion/abandonedBox | 4499 | 288 | 432 | 0.0034 | 55.93 | 0.0066 | 58.45 | 0.0077 | 26.88 | 0.0063 | 29.89 |
| intermittentObjectMotion/tramstop | 3199 | 288 | 432 | 0.0033 | 55.35 | 0.0065 | 58.66 | 0.0077 | 27.05 | 0.0065 | 29.59 |
| thermal/park | 599 | 288 | 352 | 0.0030 | 55.72 | 0.0057 | 59.96 | 0.0060 | 28.99 | 0.0056 | 33.02 |
| shadow/peopleInShade | 1198 | 244 | 380 | 0.0029 | 66.85 | 0.0053 | 74.06 | 0.0057 | 36.05 | 0.0052 | 38.74 |
| baseline/highway | 1699 | 240 | 320 | 0.0026 | 72.48 | 0.0046 | 85.70 | 0.0047 | 46.97 | 0.0040 | 53.00 |
| baseline/office | 2049 | 240 | 360 | 0.0028 | 69.49 | 0.0050 | 78.86 | 0.0051 | 40.24 | 0.0043 | 46.71 |
| baseline/pedestrians | 1098 | 240 | 360 | 0.0028 | 69.59 | 0.0051 | 78.73 | 0.0051 | 40.18 | 0.0043 | 47.00 |
| cameraJitter/boulevard | 2499 | 240 | 352 | 0.0028 | 68.96 | 0.0049 | 78.81 | 0.0051 | 41.21 | 0.0043 | 46.98 |
| cameraJitter/sidewalk | 1199 | 240 | 352 | 0.0027 | 69.04 | 0.0049 | 78.54 | 0.0050 | 39.49 | 0.0043 | 47.32 |
| cameraJitter/traffic | 1569 | 240 | 320 | 0.0026 | 72.17 | 0.0046 | 85.29 | 0.0049 | 43.95 | 0.0041 | 51.40 |
| dynamicBackground/boats | 7998 | 240 | 320 | 0.0026 | 71.86 | 0.0046 | 84.29 | 0.0045 | 45.33 | 0.0038 | 51.70 |
| dynamicBackground/canoe | 1188 | 240 | 320 | 0.0026 | 71.98 | 0.0046 | 83.86 | 0.0047 | 44.15 | 0.0039 | 52.95 |
| dynamicBackground/overpass | 2999 | 240 | 320 | 0.0026 | 71.98 | 0.0046 | 84.56 | 0.0045 | 43.69 | 0.0039 | 49.31 |
| intermittentObjectMotion/parking | 2499 | 240 | 320 | 0.0026 | 72.98 | 0.0047 | 85.21 | 0.0044 | 44.68 | 0.0038 | 48.55 |
| intermittentObjectMotion/sofa | 2749 | 240 | 320 | 0.0026 | 73.56 | 0.0046 | 86.46 | 0.0045 | 44.37 | 0.0039 | 47.96 |
| intermittentObjectMotion/streetLight | 3199 | 240 | 320 | 0.0026 | 72.01 | 0.0046 | 84.95 | 0.0045 | 44.31 | 0.0039 | 47.76 |
| intermittentObjectMotion/winterDriveway | 2499 | 240 | 320 | 0.0026 | 72.98 | 0.0047 | 85.88 | 0.0045 | 44.72 | 0.0038 | 49.21 |
| shadow/backdoor | 1999 | 240 | 320 | 0.0026 | 72.06 | 0.0046 | 85.77 | 0.0046 | 44.21 | 0.0039 | 48.87 |
| shadow/bungalows | 1699 | 240 | 360 | 0.0028 | 68.61 | 0.0050 | 78.36 | 0.0052 | 39.80 | 0.0045 | 42.25 |
| shadow/busStation | 1249 | 240 | 360 | 0.0028 | 68.79 | 0.0050 | 78.78 | 0.0053 | 39.85 | 0.0045 | 42.91 |
| shadow/cubicle | 7399 | 240 | 352 | 0.0028 | 70.87 | 0.0049 | 80.47 | 0.0050 | 41.07 | 0.0043 | 44.52 |
| thermal/corridor | 5399 | 240 | 320 | 0.0026 | 73.80 | 0.0046 | 87.01 | 0.0046 | 44.58 | 0.0039 | 48.10 |
| thermal/diningRoom | 3699 | 240 | 320 | 0.0026 | 73.38 | 0.0046 | 86.60 | 0.0048 | 44.38 | 0.0040 | 47.82 |
| thermal/lakeSide | 6499 | 240 | 320 | 0.0027 | 73.91 | 0.0047 | 86.80 | 0.0046 | 45.62 | 0.0038 | 49.64 |
| thermal/library | 4899 | 240 | 320 | 0.0027 | 74.83 | 0.0046 | 87.05 | 0.0054 | 44.40 | 0.0039 | 49.36 |

- H. Piégay, "Automated quantification of floating wood pieces in rivers from video monitoring: a new software tool and validation," *Earth Surface Dynamics*, vol. 9, no. 3, pp. 519–537, 2021.
- [35] Y. Cao, Q. Tang, X. Wu, and X. Lu, "Effnet: Enhanced feature foreground network for video smoke source prediction and detection," *IEEE Transactions on Circuits and Systems for Video Technology*, 2021.
- [36] R. Meghana, Y. Chitkara, S. Apoorva, et al., "Background-modelling techniques for foreground detection and tracking using gaussian mixture model," in *2019 3rd International Conference on Computing Methodologies and Communication (ICCMC)*, pp. 1129–1134, IEEE, 2019.
- [37] W. Kim, "Multiple object tracking in soccer videos using topographic surface analysis," *Journal of Visual Communication and Image Representation*, vol. 65, p. 102683, 2019.
- [38] B. K. Chakraborty, D. Sarma, M. K. Bhuyan, and K. F. MacDorman, "Review of constraints on vision-based gesture recognition for human-computer interaction," *IET Computer Vision*, vol. 12, no. 1, pp. 3–15, 2018.
- [39] P. K. Podder, M. Paul, and M. Murshed, "Foreground motion and spatial saliency-based efficient hevc video coding," in *2015 International Conference on Image and Vision Computing New Zealand (IVCNZ)*, pp. 1–6, IEEE, 2015.
- [40] L. Zhao, X. Zhang, X. Zhang, S. Wang, S. Wang, S. Ma, and W. Gao, "Intelligent analysis oriented surveillance video coding," in *2017 IEEE International Conference on Multimedia and Expo (ICME)*, pp. 37–42, IEEE, 2017.
- [41] H. Huang, X. Fang, Y. Ye, S. Zhang, and P. L. Rosin, "Practical automatic background substitution for live video," *Computational Visual Media*, vol. 3, no. 3, p. 1, 2017.
- [42] M. Grega, P. Donath, P. Guzik, J. Król, A. Mاتیolański, K. Rusek, and A. Dziech, "Application of logistic regression for background substitution," in *International Conference on Multimedia Communications, Services and Security*, pp. 33–46, Springer, 2017.
- [43] R. S. Dixit, S. Gandhe, and P. Dhulekar, "Pedestrian protection system for adas using arm 9," *International Journal of Computer Applications*, vol. 975, p. 8887, 2015.
- [44] P. Vasuki and S. Veluchamy, "Pedestrian detection for driver assistance systems," in *2016 International Conference on Recent Trends in Information Technology (ICRTIT)*, pp. 1–4, IEEE, 2016.
- [45] T. Chen and S. Lu, "Object-Level Motion Detection From Moving Cameras," *IEEE Transactions on Circuits and Systems for Video Technology*, vol. 27, pp. 2333–2343, nov 2017.
- [46] S. Yang, X. Hao, B. Deng, X. Wei, H. Li, and J. Wang, "A survey of brain-inspired artificial intelligence and its engineering," *Life Research*, vol. 1, no. 1, p. 23, 2018.
- [47] A. Podobas and S. Matsuoka, "Designing and accelerating spiking neural networks using opencl for fpgas," in *2017 International Conference on Field Programmable Technology (ICFPT)*, pp. 255–258, 2017.
- [48] J. Misra and I. Saha, "Artificial neural networks in hardware: A survey of two decades of progress," *Neurocomputing*, vol. 74, no. 1-3, pp. 239–255, 2010.
- [49] G. Li, V. Talebi, A. Yoonessi, and C. L. Baker, "A FPGA real-time model of single and multiple visual cortex neurons," *Journal of Neuroscience Methods*, vol. 193, no. 1, pp. 62–66, 2010.
- [50] J. Li, Y. Katori, and T. Kohno, "An FPGA-Based Silicon Neuronal Network with Selectable Excitability Silicon Neurons," *Frontiers in neuroscience*, vol. 6, p. 183, jan 2012.
- [51] A. S. Cassidy, J. Georgiou, and A. G. Andreou, "Design of silicon brains in the nano-CMOS era: Spiking neurons, learning synapses and neural architecture optimization," *Neural Networks*, vol. 45, pp. 4–26, 2013.
- [52] D. P. Moeys, T. Delbrück, A. Rios-Navarro, and A. Linares-Barranco, "Retinal ganglion cell software and fpga model implementation for object detection and tracking," in *2016 IEEE International Symposium on Circuits and Systems (ISCAS)*, pp. 1434–1437, 2016.
- [53] Q. Chen, J. Wang, S. Yang, Y. Qin, B. Deng, and X. Wei, "A real-time fpga implementation of a biologically inspired central pattern generator network," *Neurocomputing*, vol. 244, pp. 63–80, 2017.
- [54] A. O. Komendantov and N. I. Kononenko, "Deterministic chaos in mathematical model of pacemaker activity in bursting neurons of snail, helix pomatia," *Journal of theoretical biology*, vol. 183, no. 2, pp. 219–230, 1996.

TABLE IV CDnet2014 speed results.

| Category | # images | Height | Width | NeuroHSMDv1 | | NeuroHSMDv2 | | HSMDv1 | | HSMDv2 | |
|---|----------|--------|-------|-------------|-------|-------------|-------|---------|-------|---------|-------|
| | | | | SNN [s] | FPS | SNN [s] | FPS | SNN [s] | FPS | SNN [s] | FPS |
| badWeather/blizzard | 6999 | 480 | 720 | 0.0067 | 29.70 | 0.0155 | 24.55 | 0.0207 | 10.12 | 0.0174 | 11.21 |
| badWeather/snowFall | 6499 | 480 | 720 | 0.0068 | 29.61 | 0.0155 | 24.31 | 0.0203 | 10.16 | 0.0175 | 11.11 |
| badWeather/wetSnow | 3499 | 540 | 720 | 0.0074 | 26.54 | 0.0172 | 21.76 | 0.0230 | 8.93 | 0.0198 | 10.19 |
| baseline/PETS2006 | 1199 | 576 | 720 | 0.0078 | 25.04 | 0.0183 | 20.36 | 0.0250 | 8.52 | 0.0210 | 9.53 |
| cameraJitter/badminton | 1149 | 480 | 720 | 0.0068 | 28.58 | 0.0151 | 25.07 | 0.0212 | 9.80 | 0.0185 | 11.00 |
| dynamicBackground/fall | 3999 | 480 | 720 | 0.0068 | 27.48 | 0.0152 | 24.75 | 0.0170 | 13.90 | 0.0181 | 10.96 |
| shadow/copyMachine | 3399 | 480 | 720 | 0.0068 | 28.76 | 0.0152 | 25.66 | 0.0171 | 14.10 | 0.0180 | 11.51 |
| turbulence/turbulence0 | 4999 | 480 | 720 | 0.0068 | 28.59 | 0.0154 | 25.07 | 0.0165 | 14.26 | 0.0175 | 11.62 |
| turbulence/turbulence1 | 3999 | 480 | 720 | 0.0068 | 28.24 | 0.0154 | 25.21 | 0.0165 | 14.28 | 0.0175 | 11.35 |
| turbulence/turbulence3 | 2199 | 486 | 720 | 0.0069 | 28.72 | 0.0156 | 25.15 | 0.0167 | 14.07 | 0.0177 | 11.49 |
| PTZ/continuousPan | 1699 | 480 | 704 | 0.0067 | 28.49 | 0.0144 | 23.91 | 0.0235 | 9.88 | 0.0197 | 10.85 |
| lowFramerate/tunnelExit_0_35fps | 3999 | 440 | 700 | 0.0062 | 31.45 | 0.0140 | 28.23 | 0.0145 | 15.94 | 0.0153 | 12.47 |
| nightVideos/fluidHighway | 1363 | 450 | 700 | 0.0063 | 31.17 | 0.0139 | 27.64 | 0.0156 | 15.27 | 0.0164 | 12.10 |
| turbulence/turbulence2 | 4499 | 315 | 645 | 0.0045 | 41.85 | 0.0096 | 39.59 | 0.0097 | 23.90 | 0.0104 | 18.93 |
| lowFramerate/port_0_17fps | 2999 | 480 | 640 | 0.0062 | 31.35 | 0.0139 | 28.17 | 0.0149 | 15.75 | 0.0166 | 12.39 |
| lowFramerate/tramCrossroad_1fps | 899 | 350 | 640 | 0.0049 | 39.51 | 0.0104 | 36.73 | 0.0110 | 21.37 | 0.0119 | 16.71 |
| nightVideos/busyBoulevard | 2759 | 364 | 640 | 0.0050 | 38.86 | 0.0108 | 36.00 | 0.0111 | 20.90 | 0.0118 | 16.43 |
| nightVideos/bridgeEntry | 2499 | 430 | 630 | 0.0056 | 34.52 | 0.0124 | 31.85 | 0.0130 | 17.90 | 0.0135 | 14.20 |
| nightVideos/winterStreet | 1784 | 420 | 624 | 0.0055 | 35.92 | 0.0119 | 32.57 | 0.0132 | 18.26 | 0.0144 | 14.52 |
| nightVideos/streetCornerAtNight | 5199 | 245 | 595 | 0.0035 | 52.86 | 0.0074 | 51.56 | 0.0070 | 32.83 | 0.0075 | 25.35 |
| PTZ/twoPositionPTZCam | 2299 | 340 | 570 | 0.0044 | 43.30 | 0.0091 | 41.11 | 0.0125 | 17.91 | 0.0104 | 18.92 |
| PTZ/intermittentPan | 3499 | 368 | 560 | 0.0046 | 40.65 | 0.0094 | 38.52 | 0.0134 | 16.39 | 0.0114 | 17.71 |
| badWeather/skating | 3899 | 360 | 540 | 0.0044 | 43.00 | 0.0092 | 40.79 | 0.0124 | 17.20 | 0.0103 | 19.08 |
| nightVideos/tramStation | 2999 | 295 | 480 | 0.0035 | 53.15 | 0.0072 | 52.62 | 0.0071 | 33.46 | 0.0073 | 26.15 |
| dynamicBackground/fountain01 | 1183 | 288 | 432 | 0.0034 | 55.38 | 0.0066 | 57.06 | 0.0061 | 37.95 | 0.0064 | 30.16 |
| dynamicBackground/fountain02 | 1498 | 288 | 432 | 0.0034 | 56.56 | 0.0066 | 56.97 | 0.0060 | 38.22 | 0.0064 | 30.49 |
| intermittentObjectMotion/abandonedBox | 4499 | 288 | 432 | 0.0034 | 55.64 | 0.0065 | 58.03 | 0.0062 | 38.19 | 0.0065 | 30.26 |
| intermittentObjectMotion/tramstop | 3199 | 288 | 432 | 0.0034 | 56.58 | 0.0065 | 57.56 | 0.0062 | 38.03 | 0.0067 | 28.99 |
| shadow/peopleInShade | 1198 | 244 | 380 | 0.0029 | 67.31 | 0.0053 | 71.54 | 0.0046 | 49.84 | 0.0049 | 41.11 |
| baseline/office | 2049 | 240 | 360 | 0.0028 | 71.72 | 0.0050 | 75.86 | 0.0054 | 37.85 | 0.0044 | 45.39 |
| baseline/pedestrians | 1098 | 240 | 360 | 0.0028 | 70.75 | 0.0051 | 75.87 | 0.0052 | 40.13 | 0.0043 | 45.66 |
| shadow/bungalows | 1699 | 240 | 360 | 0.0028 | 69.25 | 0.0050 | 75.88 | 0.0042 | 55.53 | 0.0044 | 45.12 |
| shadow/busStation | 1249 | 240 | 360 | 0.0028 | 69.51 | 0.0050 | 74.76 | 0.0042 | 55.41 | 0.0044 | 46.24 |
| cameraJitter/boulevard | 2499 | 240 | 352 | 0.0028 | 70.44 | 0.0049 | 75.44 | 0.0053 | 39.33 | 0.0045 | 42.60 |
| cameraJitter/sidewalk | 1199 | 240 | 352 | 0.0028 | 69.44 | 0.0049 | 75.95 | 0.0052 | 38.54 | 0.0045 | 42.36 |
| shadow/cubicle | 7399 | 240 | 352 | 0.0028 | 71.78 | 0.0050 | 77.42 | 0.0041 | 57.46 | 0.0043 | 46.65 |
| thermal/park | 599 | 288 | 352 | 0.0030 | 57.07 | 0.0056 | 58.39 | 0.0049 | 43.26 | 0.0052 | 36.78 |
| PTZ/zoomInZoomOut | 1129 | 240 | 320 | 0.0026 | 72.70 | 0.0045 | 80.89 | 0.0054 | 41.94 | 0.0045 | 44.97 |
| baseline/highway | 1699 | 240 | 320 | 0.0026 | 74.12 | 0.0046 | 82.40 | 0.0051 | 42.85 | 0.0042 | 46.89 |
| cameraJitter/traffic | 1569 | 240 | 320 | 0.0027 | 72.87 | 0.0046 | 81.54 | 0.0051 | 40.97 | 0.0043 | 45.95 |
| dynamicBackground/boats | 7998 | 240 | 320 | 0.0026 | 73.14 | 0.0046 | 82.14 | 0.0038 | 60.35 | 0.0039 | 47.99 |
| dynamicBackground/canoe | 1188 | 240 | 320 | 0.0026 | 72.64 | 0.0046 | 81.62 | 0.0038 | 61.19 | 0.0041 | 46.91 |
| dynamicBackground/overpass | 2999 | 240 | 320 | 0.0027 | 72.85 | 0.0046 | 82.26 | 0.0037 | 61.72 | 0.0039 | 50.00 |
| intermittentObjectMotion/parking | 2499 | 240 | 320 | 0.0027 | 73.56 | 0.0047 | 81.88 | 0.0037 | 61.94 | 0.0038 | 51.23 |
| intermittentObjectMotion/sofa | 2749 | 240 | 320 | 0.0027 | 73.57 | 0.0046 | 82.95 | 0.0038 | 62.15 | 0.0040 | 47.82 |
| intermittentObjectMotion/streetLight | 3199 | 240 | 320 | 0.0027 | 72.77 | 0.0046 | 82.48 | 0.0037 | 62.27 | 0.0040 | 48.13 |
| intermittentObjectMotion/winterDriveway | 2499 | 240 | 320 | 0.0027 | 74.19 | 0.0047 | 82.81 | 0.0037 | 62.96 | 0.0040 | 48.48 |
| lowFramerate/turnpike_0_5fps | 1499 | 240 | 320 | 0.0026 | 73.10 | 0.0046 | 82.38 | 0.0039 | 60.99 | 0.0042 | 46.52 |
| shadow/backdoor | 1999 | 240 | 320 | 0.0026 | 73.73 | 0.0046 | 83.84 | 0.0038 | 62.82 | 0.0039 | 51.77 |
| thermal/corridor | 5399 | 240 | 320 | 0.0026 | 74.86 | 0.0046 | 83.65 | 0.0038 | 62.48 | 0.0039 | 51.11 |
| thermal/diningRoom | 3699 | 240 | 320 | 0.0026 | 74.42 | 0.0046 | 83.86 | 0.0038 | 62.34 | 0.0040 | 50.98 |
| thermal/lakeSide | 6499 | 240 | 320 | 0.0026 | 74.93 | 0.0047 | 83.60 | 0.0037 | 63.23 | 0.0038 | 51.68 |
| thermal/library | 4899 | 240 | 320 | 0.0026 | 75.79 | 0.0046 | 83.72 | 0.0038 | 62.17 | 0.0041 | 47.23 |

TABLE V CDnet2012 overall ranks.

| Method | \overline{RC} ↓ | Re ↑ | Sp ↑ | FPR ↓ | FNR ↓ | WCR ↓ | CCR ↑ | F1 ↑ | Pr ↑ |
|-------------|-------------------|------|-------|-------|-------|-------|-------|------|------|
| HSMDv1 | 1 | 0.52 | 0.994 | 0.006 | 0.23 | 0.024 | 0.976 | 0.77 | 0.62 |
| HSMDv2 | 1 | 0.52 | 0.994 | 0.006 | 0.23 | 0.024 | 0.976 | 0.77 | 0.62 |
| NeuroHSMDv1 | 1 | 0.52 | 0.994 | 0.006 | 0.23 | 0.024 | 0.976 | 0.77 | 0.62 |
| NeuroHSMDv2 | 1 | 0.52 | 0.994 | 0.006 | 0.23 | 0.024 | 0.976 | 0.77 | 0.62 |

↑: the highest score is the best.

↓: the lowest result is the best.

Re is the Recall, Sp is the Specificity, FPR is the False Positive Rate, FNR is the False Negative Rate, WCR is the Wrong Classifications Rate, CCR is the Correct Classifications Rate, Pr is the Precision, F1 is the F score or F-measure and \overline{RC} is the Average Ranking across all Categories.

TABLE VI CDnet2014 overall ranks.

| Method | \overline{RC} ↓ | Re ↑ | Sp ↑ | FPR ↓ | FNR ↓ | WCR ↓ | CCR ↑ | F1 ↑ | Pr ↑ |
|-------------|-------------------|------|-------|-------|-------|-------|-------|------|------|
| HSMDv1 | 1 | 0.55 | 0.993 | 0.007 | 0.35 | 0.018 | 0.982 | 0.65 | 0.60 |
| HSMDv2 | 1 | 0.55 | 0.993 | 0.007 | 0.35 | 0.018 | 0.982 | 0.65 | 0.60 |
| NeuroHSMDv1 | 1 | 0.55 | 0.993 | 0.007 | 0.35 | 0.018 | 0.982 | 0.65 | 0.60 |
| NeuroHSMDv2 | 1 | 0.55 | 0.993 | 0.007 | 0.35 | 0.018 | 0.982 | 0.65 | 0.60 |

↑: the highest score is the best.

↓: the lowest result is the best.

Re is the Recall, Sp is the Specificity, FPR is the False Positive Rate, FNR is the False Negative Rate, WCR is the Wrong Classifications Rate, CCR is the Correct Classifications Rate, Pr is the Precision, F1 is the F score or F-measure and \overline{RC} is the Average Ranking across all Categories.

- [55] K. Cheung, S. R. Schultz, and W. Luk, "NeuroFlow: A General Purpose Spiking Neural Network Simulation Platform using Customizable Processors," *Frontiers in Neuroscience*, vol. 9, pp. 1–15, jan 2016.
- [56] V. Sakellariou and V. Paliouras, "An fpga accelerator for spiking neural network simulation and training," in *2021 IEEE International Symposium on Circuits and Systems (ISCAS)*, pp. 1–5, 2021.
- [57] O. Community, "OpenCV," 2020. Available online, <https://opencv.org/>, last accessed 2020-01-22.
- [58] V. Samsonov, "Improvement of the background subtraction algorithm," 2017. <https://summerofcode.withgoogle.com/archive/2017/projects/6453014550282240/>, last accessed: 23/11/2020.
- [59] OpenCV, "OpenCV: Operations on arrays," 2021.
- [60] V. Samsonov, "Improved background subtraction algorithm," Nov. 2017. doi: 10.5281/zenodo.4269865, last accessed: 23/11/2020.
- [61] H. Sica De Andrade, "Thesis for The Degree of Licenciante of Engineering Software Concerns for Execution on Heterogeneous Platforms," 2018.
- [62] Kronos, "OpenCL Overview," 2021.
- [63] Intel, "Using Intel FPGA SDK for OpenCL™ on DE-Series Boards," tech. rep., Intel, 2019.
- [64] CodeProjects, "Part 5: OpenCL Buffers and Memory Affinity - Code-Project," 2011.
- [65] Intel, "Intel FPGA SDK for OpenCL Pro Edition Best Practices Guide," tech. rep., 2021.
- [66] Terasic, "Terasic - DE10-Pro," 2021. <https://www.terasic.com.tw/cgi-bin/page/archive.pl?Language=English&CategoryNo=13&No=1144&PartNo=2>, last accessed: 2021-07-31.